Journal of Applied Physics

# On channel interactions in nested Hall thrusters

Cite as: J. Appl. Phys. **123**, 133303 (2018); https://doi.org/10.1063/1.5028271
Submitted: 02 May 2017 . Accepted: 03 March 2018 . Published Online: 04 April 2018

S. E. Cusson, M. P. Georgin, H. C. Dragnea, E. T. Dale, V. Dhaliwal, I. D. Boyd, and A. D. Gallimore







AIP Publishing

JOURNAL OF APPLIED PHYSICS 123, 133303 (2018)

# On channel interactions in nested Hall thrusters

S. E. Cusson,[1,a)] M. P. Georgin,[2,b)] H. C. Dragnea,[1,c)] E. T. Dale,[1] V. Dhaliwal,[1,d)] I. D. Boyd,[1] and A. D. Gallimore[1]
[1]Department of Aerospace Engineering, University of Michigan, Ann Arbor, Michigan 48109, USA
[2]Applied Physics Program, University of Michigan, Ann Arbor, Michigan 48109, USA

(Received 2 May 2017; accepted 3 March 2018; published online 4 April 2018)

Nested Hall thrusters use multiple, concentric discharge channels to increase thrust density. They have shown enhanced performance in multi-channel operation relative to the superposition of individual channels. The X2, a two-channel nested Hall thruster, was used to investigate the mechanism behind this improved performance. It is shown that the local pressure near the thruster exit plane is an order of magnitude higher in two-channel operation. This is due to the increased neutral flow inherent to the multi-channel operation. Due to the proximity of the discharge channels in nested Hall thrusters, these local pressure effects are shown to be responsible for the enhanced production of thrust during multi-channel operation via two mechanisms. The first mechanism is the reduction of the divergence angle due to an upstream shift of the acceleration region. The displacement of the acceleration region was detected using laser induced fluorescence measurements of the ion velocity profile. Analysis of the change in beam divergence indicates that, at an operating condition of 150 V and 30 A, this effect increases the thrust by $8.7 \pm 1.2$ mN. The second mechanism is neutral ingestion from the adjacent channel resulting in a $2.0 + 0/-0.2$ mN increase in thrust. Combined, these mechanisms are shown to explain, within uncertainty, the $17 \pm 6.2$ mN improvement in thrust during dual channel operation of the X2. *Published by AIP Publishing.*
https://doi.org/10.1063/1.5028271

## I. INTRODUCTION

The Hall-effect thruster (HET) is an electric propulsion technology with moderate specific impulse and high thrust that has been primarily used for satellite station keeping and orbit raising. Improvements in solar cell technology allowing 10–100 kW of on-orbit power have enabled high-power clustered configurations such as the 40 kW solar electric propulsion system being developed by NASA's Glenn Research Center and Jet Propulsion Laboratory for the Solar Electric Propulsion Technology Demonstration Mission.[1–3] In anticipation of even higher power electric propulsion systems, the University of Michigan, in conjunction with NASA and the Air Force Research Laboratory, has investigated the concept of nested Hall thrusters (NHTs).[4,5] The NHT can offer an increased thrust density as well as an expanded operating envelope in comparison to a traditional, single channel thruster. It concentrically nests multiple discharge channels, which share a single centrally mounted cathode. Each channel can be operated individually or in any combination with the other channels. This feature gives NHTs a large throttling range compared to the traditional Hall thruster and makes it an attractive option for deep space missions. Figure 1 compares the geometry of a traditional Hall thruster and the NHT.

For missions requiring 100 kW–1 MW, NHTs are an attractive option over other high power electric propulsion systems.[6,7] The NHT is a relatively low risk technology because it is a natural extension of the HET, which has a development history dating back to the 1960s.[8] Furthermore, the nested configuration has several advantages over large clusters of Hall thrusters. The shared magnetic design leads to a lower mass-to-power ratio, and nesting results in a single thrust vector reducing the number of gimbals required for spacecraft control compared to single-channel arrays. Additionally, studies have shown that for a 1 MW system, the mass-optimized power level per thruster is between 125 and 250 kW.[7] For a 150 kW system, a NHT configuration offers a 50% reduction in the volume of the propulsion system over a cluster of HETs or 16% less mass than a single 150 kW thruster.[9]

Because the nested Hall thruster is based on the single-channel Hall thruster, it is expected that the performance characteristics and plasma properties should be similar. To establish the feasibility of the technology and explore differences between traditional and nested Hall thrusters, a two channel nested Hall thruster, the X2, was developed at the University of Michigan in conjunction with the Air Force Research Laboratory. This thruster was designed for a nominal operating voltage of 150 V at 6 kW of discharge power. To date, work has characterized thruster performance and plasma plume properties of the X2.[4,10] This initial characterization uncovered a discrepancy between the thrust produced in dual channel mode and the sum of the single channel modes. It was proposed that this discrepancy may be the consequence of enhanced neutral ingestion between the channels. Additionally, higher facility background pressure has been shown to move the acceleration region upstream, reducing the ion beam divergence angle[11] as well as the cathode

a)cusson@umich.edu
b)georginm@umich.edu
c)horatiud@umich.edu
d)Present address: Department of Mechanical Engineering, Massachusetts Institute of Technology, Cambridge, MA, 02139, USA.

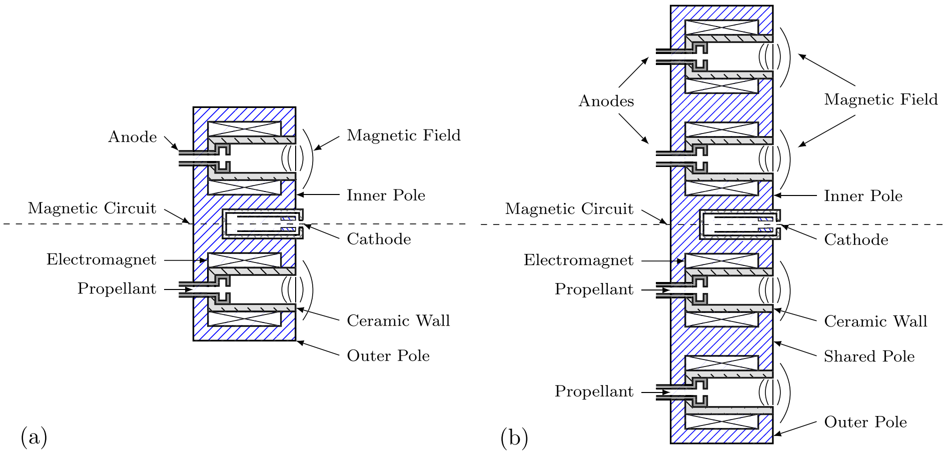


FIG. 1. Cross sectional view comparing the Hall thruster and nested Hall thruster design. The dashed line is the cylindrical axis of symmetry. (a) Schematic of a traditional Hall thruster. (b) Schematic of a nested Hall thruster with two channels.

coupling voltage.[12] A first attempt to examine this effect was made by operating at uniform background pressure; however, the discrepancy remained.[4] This result suggests that background neutral ingestion is not the cause of improved performance in nested Hall thrusters.

An important distinction is that the neutral pressure profile near the face of the thruster is significantly different between dual and single channel operation. The difference in the local pressure profile could be affecting thruster performance. In traditional Hall thrusters, additional facility pressure can result in an improved mass utilization efficiency.[13–15] While previous works investigated far-field facility induced pressure changes, near-field thruster-induced pressure changes could feasibly follow similar patterns. This study investigates how the difference in the local pressure profile between multi-channel and single channel operation results in additional neutral ingestion and reduced divergence angle in a nested Hall thruster.

To show that these local pressure effects are the dominant processes by which thrust increases in the X2, the experiment was designed such that the facility background pressure was kept constant for all test points while the local pressure was varied. The presence of these phenomena induced by the local pressure profile was investigated through performance, current density, divergence angle, and acceleration region measurements.

## II. EXPERIMENTAL APPARATUS

### A. Nested Hall thruster and vacuum facility

The X2 nested Hall thruster was used for this study of local pressure effects. Initially developed as a proof-of-concept for nesting discharge channels concentrically, the thruster features two discharge channels of similar anode design and magnetic field topographies. The thruster operates as an $E \times B$ discharge. The thruster uses a magnetic lens topography,[16] similar to other state-of-the-art Hall thrusters. Due to shared magnetic components, the magnetic field on the inner channel points radially inward while the outer channel magnetic field points radially outward. The channels share a single centrally mounted $LaB_6$ hollow cathode. A picture of the thruster during firing and after fabrication is shown in Fig. 2.

All experiments took place in the Large Vacuum Test Facility (LVTF) at the University of Michigan. The chamber is nine meters long and six meters in diameter, and uses four mechanical pumps and seven cryogenic pumps with a pumping speed of 240 000 L-Xe/s to achieve base pressures of $1 \times 10^{-7}$ Torr – $N_2$. The facility uses Varian Series UHV-564 ion gauges to measure pressure at the chamber wall approximately one meter downstream of the thruster. The chamber pressure was $6.8 \times 10^{-6}$ Torr-Xe during operation. The X2 was operated at 150 V and 4.5 kW of total discharge power. The discharge power of the inner and outer channels was 1.25 kW and 3.25 kW, respectively. Each channel was run off separate, commercially available power supplies. If a channel was not being operated, i.e., during single channel operation, that channel's power supply was not activated. Six commercially available power supplies were used to power the cathode heater, keeper, and electromagnets. The thruster was supplied with research grade xenon via three commercially available mass flow controllers. An additional mass flow controller delivered research grade xenon downstream to artificially increase the background pressure during single channel operation. The mass flow was 21.8 mg/s for the outer channel and 8.7 mg/s for the inner channel. The cathode flow fraction was kept at a constant 10% of the anode flow rate for all activated channels. This implies that the cathode flow rate was the same for all cases in which the same channels had plasma discharges. Throughout the experiments, the thruster body was electrically connected to

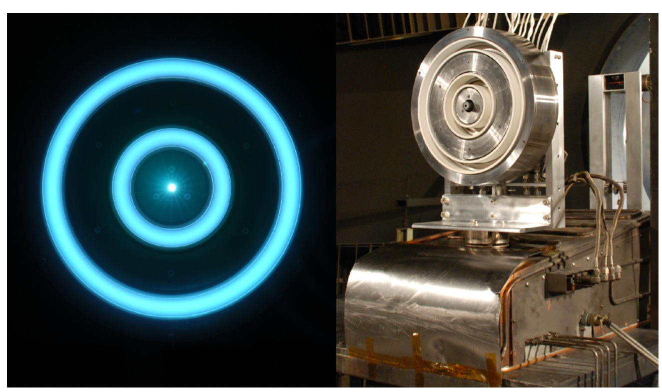

FIG. 2. The X2 Hall thruster shown operating at 4.5 kW (left) and installed on the thrust stand (right).

chamber ground. The applied magnetic field strength for each operating condition was identical.

### B. Pressure profile measurement

The local pressure profile for each operating condition was measured using a Varian Stabil Series 370 ionization gauge during cold flow testing of the X2. The ionization gauge was placed 0.35 $d_{OC}$ downstream of the thruster exit plane with its entrance perpendicular to the direction in the flow. Figure 3 illustrates the test setup.

The thruster was placed on motion stages such that a radial sweep of the pressure profile could be measured. The mass flow rate during this measurement was the same as during thruster operation. The local pressure profile was used to determine the neutral density near the thruster exit plane.

Additionally, this number density profile was confirmed via numerical simulation. The two-dimensional axisymmetric simulation of xenon neutral particles was performed using the computer code Monaco,[17] which is an implementation of the direct simulation Monte Carlo method (DSMC).[18] Two separate xenon species are defined based on their origin, which enables the tracking of xenon particles injected in the inner and outer channels. There are two inflow conditions: one at the inner channel anode and one at the outer channel anode. A wall condition is implemented at the thruster channel walls, and a line of symmetry is located on the downstream plume boundary. The north and east domain boundaries enforce an outflow outflow which allows particles to leave the domain.

### C. Thrust stand

An inverted pendulum thrust stand, similar to that described by Walker,[19] was used to perform thrust measurements. The stand features a one newton range with an approximate 4 mV/mN sensitivity. It was run in null mode, and multiple calibrations were done after each thrust measurement to reduce uncertainty. The thrust stand uses an electromagnetic coil controlled by a proportional, integral, derivative (PID) controller to maintain position. During this experiment, the thrust data had a one hertz low amplitude oscillation superimposed on the data due to PID tuning. This oscillation was filtered out during data post-processing. The uncertainty of the thrust data was taken as the standard deviation of the thrust signal which was typically 1%–2% of the value. The last five minutes of thrust data was averaged together to get the thrust value.

### D. Faraday probe

A near-field Faraday probe was used to measure beam current as a function of radial and axial location. The design of the Faraday probe features a tungsten planar disk of 3.2 mm diameter. There is also an outer guard ring in order to reduce edge effects, as described by Rovey.[20]

The probe was biased to $-40$ V during operation to ensure ion saturation. Per standard practice, the guard ring was also biased to $-40$ V. The probe was placed on two-dimensional motion stages. Several radial scans were taken at axial locations ranging from 0.07 $d_{OC}$ to 0.17 $d_{OC}$ downstream of the thruster. During each sweep, the probe was continuously moving and the position profile was recorded versus time. Current was measured using a Keithley 6485 picoammeter sampling at 60 Hz.

### E. Laser-induced fluorescence

A non-resonant laser-induced fluorescence technique was used to measure the ion velocity distribution functions (IVDFs) in the acceleration region of the X2. Laser-induced fluorescence has been used extensively to measure IVDFs in the Hall thruster plume and channel.[21–26] In this work, axial IVDF measurements were collected at several axial positions along the centerline of each channel. These measurements were made possible by mounting the thruster to the radial-axial motion stages. The collection volume was 1 $mm^3$, and the laser power at the point of interrogation was between 40 and 70 mW, depending on the quality of the coupling into the vacuum facility. The transition of $Xe^+$ used for IVDF measurements was the 834.9 nm line.

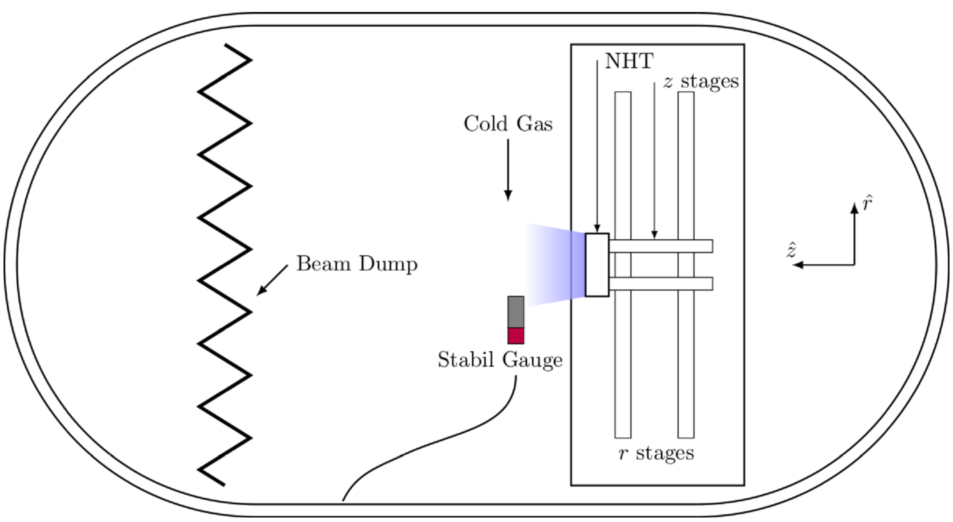


FIG. 3. Schematic for the test setup of cold flow testing. The thruster was on motion stages and the Stabil-Ion Gauge was pointed perpendicular to the flow downstream of the exit plane.

## III. EXPERIMENTAL METHODS

The goal of this experiment was to investigate how the difference in the local pressure profile between single and multi-channel modes might result in improved thruster performance. To match the facility background pressure of the multi-channel mode while operating in single channel mode, xenon gas was injected via a downstream gas injector. To match the background pressure and approximately match the local pressure, gas was also injected via the inactive channel. Figure 4 illustrates the five resulting operating conditions: (1) dual channel operation, (2) inner channel operation with downstream injection, (3) inner channel operation with outer channel injection, (4) outer channel operation with downstream injection, and (5) outer channel operation with inner channel injection.

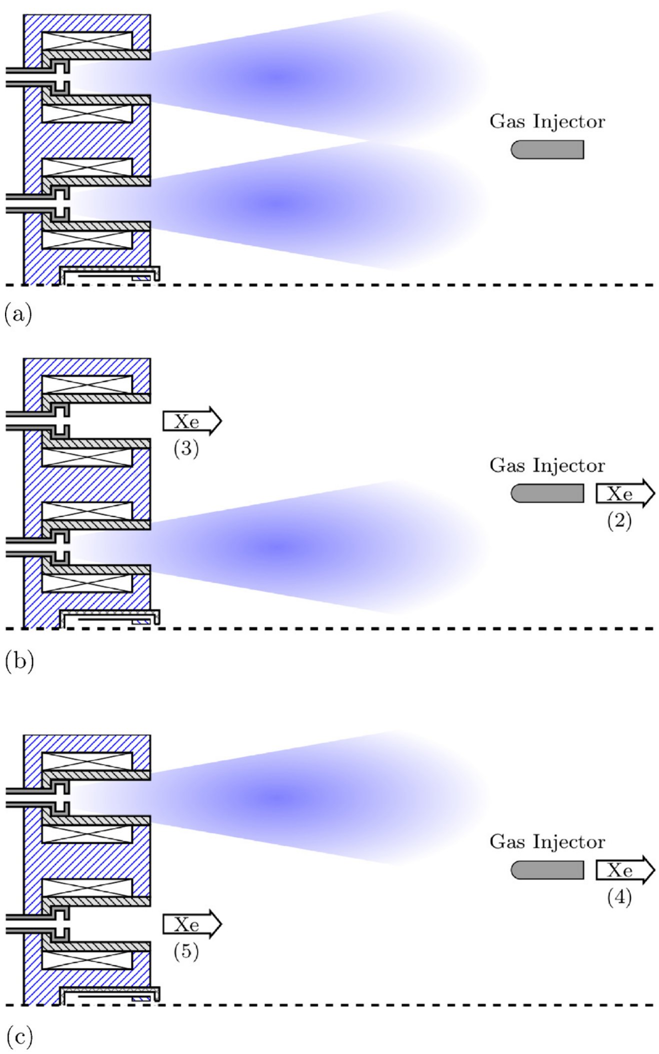


FIG. 4. Schematic of the thruster operating conditions. For all conditions, the discharge voltage was 150 V and the applied magnetic field strength was identical. The five operating conditions results are detailed above. Injection here is referring to neutral gas injection to match the facility pressure. (a) Multi-channel operation (1) is shown where there is no additional gas injection. (b) Test conditions involving inner channel operation with downstream gas injection (2) to match background pressure and outer channel gas injection (3) to match background and local pressure. (c) Test conditions involving outer channel operation with downstream gas injection (4) to match background pressure and inner channel gas injection (5) to match background and local pressure.

When cold gas flows through the thruster, it produces a non-negligible amount of thrust. During channel injection, test points 3 and 5, there was cold gas flowing through the non-operational channel. The thrust due to cold gas flow was approximated as

$$F_{th,cold\,gas} = \dot{m} v_{th}, \tag{1}$$

$$v_{th} = \sqrt{\frac{8kT_{gas}}{\pi m_{Xe}}}, \tag{2}$$

where $\dot{m}$ is the mass flow through the non-operating channel, $v_{th}$ is the thermal velocity, $k$ is Boltzmann's constant, $T_{gas}$ is the temperature of the gas, and $m_{Xe}$ is the mass of a xenon atom. The temperature in Eq. (2) was assumed to be 600 K, the approximate steady state temperature of the thruster during operation. The thrust due to cold gas from the inner and outer channels was calculated to be 3 mN and 7 mN, respectively. These estimates were subtracted out of the total thrust. Additionally, experimental data presented by Cusson[27] are utilized here as well as previously unreported data.[28,29]

## IV. THEORY

In order to quantify what the expected results from this experiment are, we present the following theory. Previously, it has been assumed that the thrust in multiple channel operation is simply the sum of the two channels operating alone. However, results[4] suggest that this is not the case, even when background pressure is accounted for. Here, we present the theory that the local pressure profile of a NHT is the dominant mechanism by which anomalous thrust is produced. The increased neutral density near the thruster will lead to two mechanisms of improved performance: (1) neutral ingestion resulting in a higher beam current and (2) acceleration region movement resulting in a lower divergence angle. Neutral ingestion is a well-documented phenomenon in Hall thrusters.[11,14,15] Frieman[30] showed that the ingested mass flow rate due to background neutrals should be

$$\dot{m}_{ing} = \Phi m A_{exit}, \tag{3}$$

where $m$ is the mass of the xenon atom, $A_{exit}$ is the thruster exit area, and $\Phi$ is the flux of background particles found to be[30]

$$\Phi = \frac{1}{4} n_b \sqrt{8kT_b/\pi m}. \tag{4}$$

Here, $n_b$ is the number density of background neutrals, $k$ is Boltzmann's constant, and $T_b$ is the temperature of the background neutrals. Assuming that this model can be extended to neutral ingestion from a proximal source, the thrust addition due to neutral ingestion should be

$$F_{ingestion} = \dot{m}_{ing} u_e P_i, \tag{5}$$

where $u_e$ is the exit velocity of the ionized ingested particles and $P_i$ is the ionization fraction of the ingested particles. To estimate the contribution of channel ingestion, the neutral density near the thruster exit and ion exit velocity is measured. Additionally, laser induced fluorescence (LIF) provides insight into movement of the acceleration region.

With increasing background pressure, experimental measurements have shown that the acceleration region of a Hall thruster will shift upstream.[11,28] If a shift in the acceleration region is measured at constant background pressure in a nested configuration, then the change in local pressure is likely affecting the divergence of the ion beam. The thrust divergence efficiency for a single channel is given by[31]

$$\eta_t = \frac{\int_{r_1}^{r_2} 2\pi r j(r)\cos(\theta) dr}{I_b}, \tag{6}$$

where $\eta_t$ is the thrust divergence efficiency, $j(r)$ is the current density distribution, $r_1$ and $r_2$ are the radial location of the 90% bounds for current density, $\theta$ is the half-angle divergence, and $I_b$ is the total beam current. It can easily be seen that the theoretical thrust without divergence losses (a divergence of zero), $F_{zero,div}$, is calculated as $F_{actual} = \eta_t F_{zero,div}$. $F_{actual}$ is the measured thrust. The beam current is calculated as

$$I_b = \int_0^{2\pi}\int_{r_1}^{r_2} j(r,z) r dr d\phi, \tag{7}$$

where $\phi$ is the azimuthal angle around the thruster about thruster centerline. To compute the total thrust divergence efficiency of both channels, the efficiencies are multiplied together[31]

$$\eta_t^{tot} = \eta_t^{inner}\eta_t^{outer}. \tag{8}$$

Additionally, the increased thrust due to an increase in divergence efficiency is the difference in thrust losses between single-channel and dual channel mode. Since the thrust losses in any given mode are $(1-\eta_t)F_{zero,div}$, the increased thrust, $F_{div}$ is

$$F_{div} = (1-\eta_1)F_1 - (1-\eta_2)F_2, \tag{9}$$

where $\eta_2$ is the divergence efficiency in dual channel, $\eta_1$ is the divergence efficiency in single channel mode, $F_2$ is the calculated thrust before divergence losses in dual channel mode, and $F_1$ is the summation of the calculated thrust before divergence losses for the inner and outer channels in downstream injection mode. Combining all this, the expected thrust of the device in multi-channel operation is

$$F = F_{inner} + F_{outer} + F_{ingestion} + F_{div}, \tag{10}$$

where $F_{inner}$ is the measured thruster for the inner channel in downstream injection mode and $F_{outer}$ is the measured thruster for the outer channel in downstream injection mode.

## V. RESULTS AND DISCUSSION

### A. Performance

#### 1. Efficiency analysis

The signal from the thrust stand described in Sec. II C was used to find the thrust produced by the X2 at each of the operating conditions. Anode efficiency and specific impulse were then calculated from thrust measurements as

$$\eta_a = \frac{T^2}{2\dot{m}_a P_d}, \tag{11}$$

$$I_{sp,a} = \frac{T}{\dot{m}_a g}, \tag{12}$$

where $\eta_a$ is the anode efficiency, $T$ is the thrust, $\dot{m}_a$ is the total anode mass flow rate, $P_d$ is the discharge power, $I_{sp,a}$ is the anode specific impulse, and $g$ is the gravitational acceleration. When the thruster is running in dual channel mode, it is not possible to deconvolve the thrust of each individual channel. Therefore, in an effort to compare the performance in dual channel mode and the combination of single channel modes, effective performance properties are defined. This effective performance gives the expected dual channel results based on single channel results. It is calculated as

$$\eta_{effective} = \frac{(T_{inner} + T_{outer})^2}{2\dot{m}_a(P_{inner} + P_{outer})}, \tag{13}$$

$$I_{sp,effective} = \chi_{inner} I_{sp,inner} + \chi_{outer} I_{sp,outer}, \tag{14}$$

$$\chi_{inner} = \frac{\dot{m}_{inner}}{\dot{m}_a} \quad \chi_{outer} = \frac{\dot{m}_{outer}}{\dot{m}_a}. \tag{15}$$

This can be calculated for any single channel condition (channel injection or downstream injection), for which, the respective inner and outer quantities would be used in Eqs. (13) through (15).

#### 2. Thrust and specific impulse

After the analysis above, the resulting thrust is calculated as shown in Table I. The table includes the test point, the resulting channels operating, thrust, power, and the location of gas injection if applicable. At the bottom of the table is the summation of inner and outer channels with downstream injection and channel injection for comparison to dual channel results. The results show that the thrust in dual channel mode (357.8 mN) is 17 mN higher than the thrust resulting from the summation of single channel operation with downstream injection (340.8 mN) when operating at the same background pressure. This 17 mN corresponds to a 5% increase in thrust. However, when the pressure is matched via channel injection, this discrepancy is eliminated within the uncertainty of the measurement (total thrust is 358.9 mN). This suggests that the presence of more neutrals

TABLE I. Thrust results at all test points and injection location for reference.

| Test point | Channels operating | Thrust (mN) | Power (kW) | Injection location |
|---|---|---|---|---|
| 1 | Dual channel | $357.8 \pm 4.5$ | $4.46 \pm 0.08$ | N/A |
| 2 | Inner channel | $92.7 \pm 2.7$ | $1.26 \pm 0.05$ | Downstream |
| 3 | Inner channel | $94.5 \pm 3.0$ | $1.27 \pm 0.05$ | Outer channel |
| 4 | Outer channel | $248.1 \pm 3.3$ | $3.26 \pm 0.08$ | Downstream |
| 5 | Outer channel | $264.8 \pm 3.6$ | $3.24 \pm 0.07$ | Inner channel |
| 1 + 3 | Summation downstream | $340.8 \pm 4.3$ | $4.52 \pm 0.09$ | Downstream |
| 2 + 4 | Summation channel injection | $358.9 \pm 4.7$ | $4.51 \pm 0.09$ | Channels |

TABLE II. Effective anode efficiency, specific impulse, and total thrust for the single channel modes versus dual channel mode.

| Test point | (Effective) Anode efficiency | (Effective) $I_{sp,a}$ (s) | Thrust (mN) | Note |
|---|---|---|---|---|
| 1 (Dual channel) | 0.47 ± 0.01 | 1196 ± 14 | 357.8 ± 4.5 | Measured |
| 2 + 4 (Downstream) | 0.42 ± 0.02 | 1141 ± 33 | 340.8 ± 4.3 | Calculated |
| 3 + 5 (Channel) | 0.47 ± 0.03 | 1204 ± 36 | 358.9 ± 4.7 | Calculated |

in the vicinity of the thruster is resulting in higher thrust. A similar trend is observed in the effective efficiency and specific impulse shown in Table II. The results show that when the pressure is controlled via downstream injection, the efficiency and specific impulse of the thruster is lower than in dual channel mode; however, when the pressure is matched with channel injection, the performance is nearly identical to dual channel mode. This indicates that the increased neutral density near the thruster is causing the increased performance. However it does not reveal the mechanism by which this occurs. In Sec. IV, a change in the divergence of the ion beam and neutral ingestion from the other channel are identified as possible processes by which the performance of the thruster is improved.

Faraday probe data are shown in Fig. 5. These data are used to determine thrust improvement due to divergence changes. Additionally, to determine the thrust increase due to ingestion, the neutral density profile is used to determine neutral density (as discussed in Sec. II B) and laser induced fluorescence is used to determine exit velocity. Results are shown in Secs. V B and V D 2.

## B. Divergence angle

The current density across the face of the X2 was measured using the near-field Faraday probe described in Sec. II D. An example of the measured current density profile can be seen in Fig. 5. Using the measured current density profile, the divergence angle of the ion beam was then calculated as

$$\theta(z) = \arctan\left(\frac{r_2 - r_{max}}{z}\right), \tag{16}$$

where $\theta(z)$ is the divergence angle at an axial location $z$, $r_{max}$ is the radial location of the maximum current density, and $r_2$ is the radial location of the cutoff point. The selection of the cutoff point is discussed below. Due to the nature of nested Hall thrusters, it is necessary to take near-field Faraday probe measurements to distinguish the channels from each other prior to plume merging. To avoid the effects of plume merging, the radial cutoff limit $r_2$ was set to the 1/e dropoff point of the maximum at each axial location as described by Reid.[32] Equation (16) was used to calculate the divergence angle until the downstream location in which plume merging made it impossible to differentiate the cathode plume, the inner channel plume, and the outer channel plume from each other. Error is estimated through the range of multiple measurements.

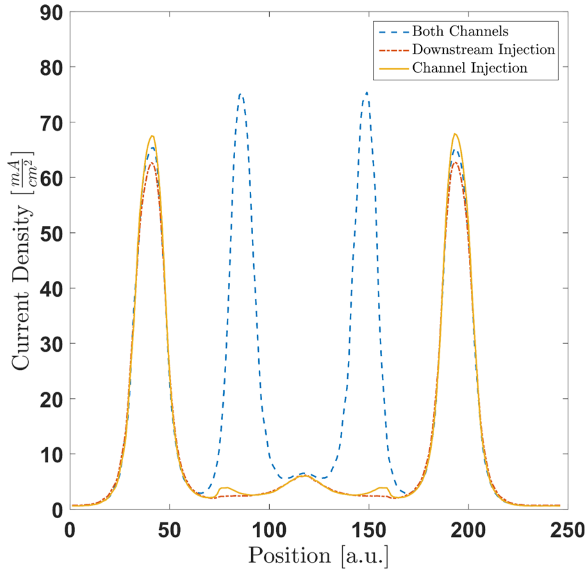


FIG. 5. Example current density trace showing the outer channel for all three cases (dual, downstream injection, and inner channel injection).

The divergence angle as a function of axial location is shown in Fig. 6. These measurements indicate that the divergence angle in dual channel mode is consistently lower than single channel mode when pressure is matched via downstream injection. Furthermore, when the local pressure profile is approximately matched through channel injection, the ion beam diverges less than during downstream injection. During channel injection, the ion beam divergence of the outer channel matches, within uncertainty, the divergence of

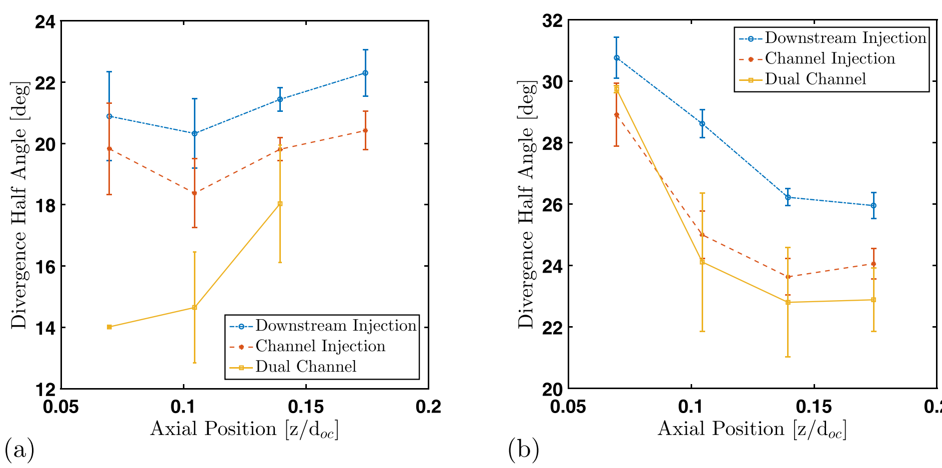


FIG. 6. Divergence angle as a function of downstream position; all axial positions are normalized by the outer channel diameter ($d_{OC}$). (a) Inner channel divergence angle as a function of downstream position. (b) Outer channel divergence angle as a function of downstream position.

TABLE III. Beam current values for high power operation.

| Test point | Test condition | Beam current (A) |
|---|---|---|
| 2 | Inner channel w/downstream injection | 7.63 ± 0.08 |
| 3 | Inner channel w/channel injection | 7.74 ± 0.04 |
| 4 | Outer channel w/downstream injection | 20.24 ± 0.10 |
| 5 | Outer channel w/channel injection | 20.77 ± 0.01 |
| 1 | Dual channel | 28.35 ± 0.31 |
| 3 + 5 | Channel injection summation | 28.51 ± 0.05 |
| 2 + 4 | Downstream injection summation | 27.87 ± 0.13 |

TABLE IV. Divergence efficiency for the single channel modes versus the dual channel mode.

| Test point | Divergence efficiency |
|---|---|
| 1 (dual channel) | 0.872 ± 0.001 |
| 2 + 4 (downstream) | 0.840 ± 0.001 |
| 3 + 5 (channel) | 0.864 ± 0.004 |

the outer channel in dual channel mode. This suggests matching local pressure better predicts dual channel divergence. For the inner channel, the very-near-field dual channel and channel injection divergence angles do not match. In dual channel operation, the cathode plasma is significantly denser due to the increased current and flow rate required for operation. This in turn could reduce the cathode to inner channel plasma density gradient resulting in a lower divergence in the near-field, as suggested by Hofer.[33] However, they still evolve to the same value below that of the downstream injection divergence angle.

The beam current was also calculated from the near-field Faraday probe in order to analyze divergence efficiency. Using Eq. (7), the beam currents are calculated and shown in Table III. From Table II, the thrust in dual channel mode is 17 mN greater than the sum of the single channels with downstream injection. Using the beam current and Eq. (6), the divergence efficiency was calculated and can be seen in Table IV. From these results, and using Eq. (9), it can be seen that going from single channel (downstream injection) to dual channel mode would result in an $8.7 \pm 1.2$ mN increase in thrust. Therefore, we conclude that not only does the divergence angle change but it also accounts for about half the improvement in thrust during dual channel operation. However, this result also suggests that the reduced divergence angle is not the only mechanism behind improved performance. Furthermore, it does not reveal the mechanism behind the changing divergence angle, to be discussed in Sec. V D.

### C. Local pressure profile

Results for cold flowing xenon from the radial sweeping of a Stabil-Ion Gauge in front of the thruster are shown in Fig. 7(a). The results indicate that with a base pressure of $5.1 \times 10^{-7}$ Torr-Xe the maximum pressure in dual-channel mode at axial location $z = 0.35\ d_{OC}$ from the exit plane is $1.4 \times 10^{-4}$ Torr-Xe, while the maximum pressure with downstream injection is $8.7 \times 10^{-5}$ Torr-Xe for both the inner and outer channels. The pressure profile for dual-channel mode qualitatively matches the sum of the single-channel test cases because the same flow is being injected into the chamber in the same locations. The total flow into the chamber when summing the two profiles is higher because of two effects that are included twice: the cathode flow and the background pressure. Therefore, the pressure magnitude is higher than in the dual channel case. The cathode flow is added twice because the center-mounted cathode is shared between the two channels. The background pressure is added twice because in both single channel cases we are matching the same background pressure by additional neutral injection; however, this effect is smaller in magnitude than that of the cathode flow (an order of magnitude smaller). Since this measurement does not account for ionization, these results cannot definitively confirm the validity of this technique. However, they suggest that pressure from single channel modes can be approximately summed to compare to dual channel values. These data show that neutral density near the thruster is much higher in dual channel mode than in any of the two single channel modes even when the background pressure is the same.

Figure 7(b) shows that the simulation confirms, to order of magnitude, the experimental results. There are a few quantitative differences in the plots, such as the maximum magnitude for the outer channel profile. This can be reasonably explained by the consideration that the simulation data is tracking inner and outer particles separately for a dual channel condition. Conversely, the measured data show each channel individually and then operating together. There is no way to differentiate species coming from the inner channel versus the outer channel for dual channel experimental

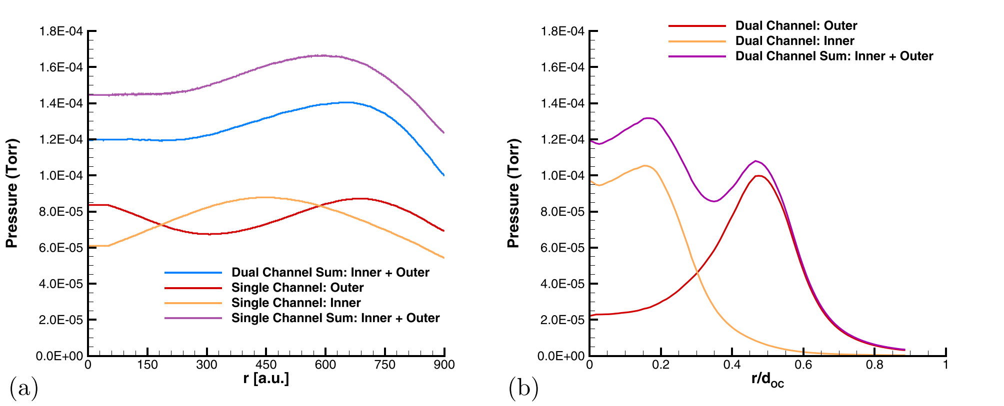


FIG. 7. Cold flow radial pressure maps from (a) experiments and (b) simulation. (a) shows the neutral pressure profile for firing condition 2 (yellow), condition 4 (red), and condition 1 (blue). It also shows the summation of conditions 2 and 4 (purple). Conditions 3 and 5 are not explicitly shown because during cold flow testing, they would appear the same as condition 1. Numerical modeling results for dual channel neutral flow without back pressure are shown in (b), with labels based on the origin of the xenon species. (a) Experimental. (b) Computational.

measurements. Additionally, there is the presence of the background pressure during experiments.

Assuming that the xenon neutrals are at 300 K (no plasma present to heat the neutrals), the density of the inner channel neutrals diffusing to the outer channel centerline (at $z = 0.35\ d_{OC}$) is calculated from the DSMC simulation to be $5.7 \times 10^{17}\ \mathrm{m^{-3}}$, while the density of the outer channel neutrals diffusing to the inner channel centerline is $1.2 \times 10^{18}\ \mathrm{m^{-3}}$. The typical ionization fraction in Hall thrusters is approximately 15%;[34] therefore, the neutral density near the channel would only be 85% of the calculated density. These values, in conjunction with Eq. (5), are used to calculate thrust due to ingestion.

### D. Laser induced fluorescence

Below are the results from the laser induced fluorescence (LIF) experiment. First, we present a physical picture of our expectation for the shape of the IVDFs that provides context and guides our analysis. Then, we analyze the results through curve fitting of the data and computing moments of the IVDFs to find bulk properties of the plasma in the acceleration region.

#### *1. Physical picture*

In the channel of the Hall thruster, the two primary processes that determine the spatial evolution of the IVDF are ionization and electrostatic acceleration.[35,36] Upstream of the acceleration region, ions are formed in the primary ionization region by electron impact ionization with an approximately Maxwellian IVDF.[8] However, there is typically some overlap between the ionization and acceleration regions.[36] Local ionization results in a signal at $v = 0$ while the electric field produces a second accelerated population. This leads to the conclusion that in general we expect to find IVDFs with two ion populations in the acceleration region.

Not only do we expect there to be two ion populations but we also expect those distributions to be skewed because of the electric field in the acceleration region. First, we will motivate the skewness of the locally ionized population in the acceleration region. The ions generated just upstream of an LIF interrogation point will be slightly accelerated because of the electric field. This causes the locally ionized population to appear skewed toward positive velocities. The skewness of the ion beam population is a direct result of overlap between the ionization region and the acceleration region. Since some ions are formed after the primary ionization region, they will receive less kinetic energy as they do not travel through the full accelerating potential. Therefore, the ion beam population will skew towards lower velocities. In summary, based on this physical picture, we expect to observe IVDFs with two populations where each population is skewed towards the other. IVDFs similar to the expectation we have developed are widely reported in the literature.[11,26,37,38]

#### *2. Analysis technique*

Using the physical picture above, we expect that the data should be well represented by the sum of two skewed Maxwellian functions. The function used to fit the IVDFs was

$$f(v,z) = \sum_{i=1}^{2} a_i(z)\left(1 + \mathrm{erf}\left(\alpha_i(z)\frac{v - v_i(z)}{\sqrt{2}\sigma_i(z)}\right)\right) \times \exp\left(-\frac{(v - v_i(z))^2}{2\sigma_i(z)}\right), \tag{17}$$

where $a_i(z)$, $\alpha_i(z)$, $v_i(z)$, and $\sigma_i(z)$ are the fit parameters and $v$ is our random variable. $a_i(z)$ represents the amplitude of the $i$th distribution. $v_i(z)$ represents the mean velocity of the distribution at the location $z$ in the plume. $\alpha_i$ controls the skewness of the distribution and $\sigma_i$ controls the variance. In the following analysis, the first term, $i = 1$, is referred to as the locally ionized population and the second term, $i = 2$, as the ion beam population.

Equation (17) is used to curve fit the raw IVDFs. From this curve fit, we extract the most probable velocity of the ion beam and compute the first moment of the full IVDF to find the mean ion velocity. This analysis works well when the two populations are distinct. However, in the ionization region, the populations overlap and cannot be distinguished. In these cases, we fit a single skewed Maxwellian distribution and estimate the velocity of the ion beam to be the mean velocity. This is found by computing the first moment of the IVDF. The variance in the most probable and mean velocity is found by under-sampling the IVDF data, refitting it with Eq. (17) and recomputing the first moment.

#### *3. Outer channel*

Figure 8 shows the ion beam velocity as a function of position using the technique described in Sec. V D 2. The position and length of the acceleration region were estimated by curve fitting the velocity curves to the complementary error function shown in the following equation:

$$v(x) = \frac{v_{max}}{2}\,\mathrm{erfc}\left(\frac{x_0 - x}{\ell}\right). \tag{18}$$

Here, $v_{max}$ is the ion velocity after acceleration, $x_0$ is the center of the acceleration region, and $\ell$ is the length of the acceleration region. A distinct shift and compression of the acceleration region is observed when the local pressure is matched using channel injection. Lastly, the exit velocities at 12 mm downstream of the exit plane for the dual channel and channel injection conditions are greater than during downstream gas injection. The shift and compression of the acceleration region as well as the exit velocities are summarized in Table V.

#### *4. Inner channel*

Figure 9 shows the ion beam velocity curve for the inner channel. The dual channel and channel injection conditions have their acceleration regions compressed and shifted upstream compared to the downstream injection condition and the exit velocities at 12 mm downstream of the exit plane are greater. However, matching the local pressure with

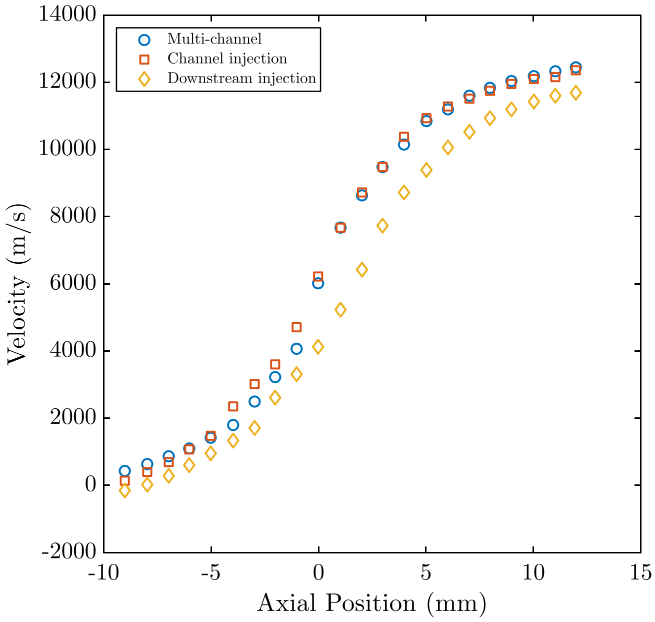


FIG. 8. Comparison of ion beam velocity curves for each condition along the outer channel.

TABLE V. Length and position of the acceleration region and ion beam exit velocity at 12 mm for the outer channel.

| Test point | Length (mm) | Position w.r.t. the exit plane (mm) | Exit velocity (m/s) |
|---|---|---|---|
| Dual channel | $4.5 \pm 0.2$ | $2.3 \pm 0.2$ | 12 500 |
| Downstream injection | $4.75 \pm 0.09$ | $3.67 \pm 0.09$ | 11 700 |
| Channel injection | $4.6 \pm 0.1$ | $2.1 \pm 0.1$ | 12 400 |

channel gas injection does not precisely replicate dual channel operation.

#### 5. Discussion

The analysis of the LIF has shown that increasing local pressure results in an upstream shift of the acceleration region. A similar relationship was also shown by Nakles with the facility background pressure.[11] When the acceleration region is shifted up-stream, the discharge is confined more by the walls. Therefore, the expectation is that the divergence of the ion beam should be reduced. The divergence angle measurements in Sec. V B have shown that an increase in local pressure reduces the divergence angle of the thruster which increases the thrust at constant discharge current. The combination of the divergence angle and IVDF measurements shows that a change in the local pressure shifts the acceleration region leading to a reduced divergence angle and improved thrust.

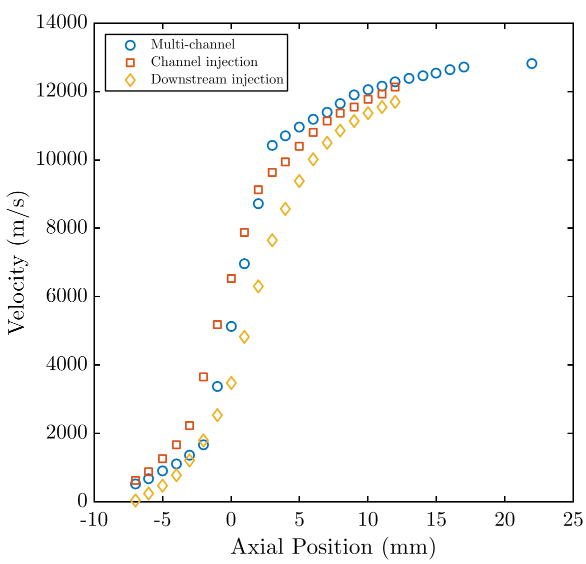


FIG. 9. Comparison of ion beam velocity curves for each condition along the inner channel. Position = 0 is the exit plane of the X2.

TABLE VI. Length and position of the acceleration region and ion beam exit velocity at 12 mm for the inner channel.

| Test point | Length (mm) | Position w.r.t. exit plane (mm) | Exit velocity (m/s) |
|---|---|---|---|
| Dual channel | $3.3 \pm 0.2$ | $2.2 \pm 0.2$ | 12 300 |
| Downstream injection | $4.0 \pm 0.2$ | $3.6 \pm 0.1$ | 11 700 |
| Channel injection | $3.8 \pm 0.3$ | $1.3 \pm 0.3$ | 12 100 |

### E. Ion exit velocity

As shown in Tables V and VI, ion exit velocity at 12 mm downstream of the exit plane increases in the dual channel and channel injection conditions by about 500 m/s compared to the downstream injection case. Therefore, the beam current should increase correspondingly. However, a more appropriate parameter to use for comparison is the mean ion exit velocity since all ions are being collected by the near-field Faraday probe. The mean exit velocities are shown in Table VII.

Parallel to the analysis in Sec. V A 2, an average weighted by the mass flow rates can be used to discuss global properties of a nested Hall thruster. The computed average exit velocities in Table VII along with Eqs. (3), (4), and (5) are used to estimate the additional thrust due to neutral ingestion. Assuming an ionization fraction of $15^{+0}_{-5}\%$,[34] the estimated improvement in thrust was computed to be $2.0^{+0}_{-0.2}$ mN.

#### 1. Interaction by discharge oscillations

Hall thruster discharges generally sustain low frequency, 10 kHz to 1 MHz, oscillations and the literature has shown that these oscillations can affect thruster performance.[38–43] Whether these oscillations improve or diminish thruster

TABLE VII. Mean exit velocities for both channels at 12 mm downstream of the exit plane.

| Test point | Channel | Mean exit velocity (m/s) |
|---|---|---|
| Dual channel | Inner | $9100 \pm 200$ |
| Downstream injection | Inner | $9800 \pm 300$ |
| Channel injection | Inner | $9600 \pm 200$ |
| Dual channel | Outer | $10\,400 \pm 100$ |
| Downstream injection | Outer | $10\,200 \pm 200$ |
| Channel injection | Outer | $10\,900 \pm 100$ |

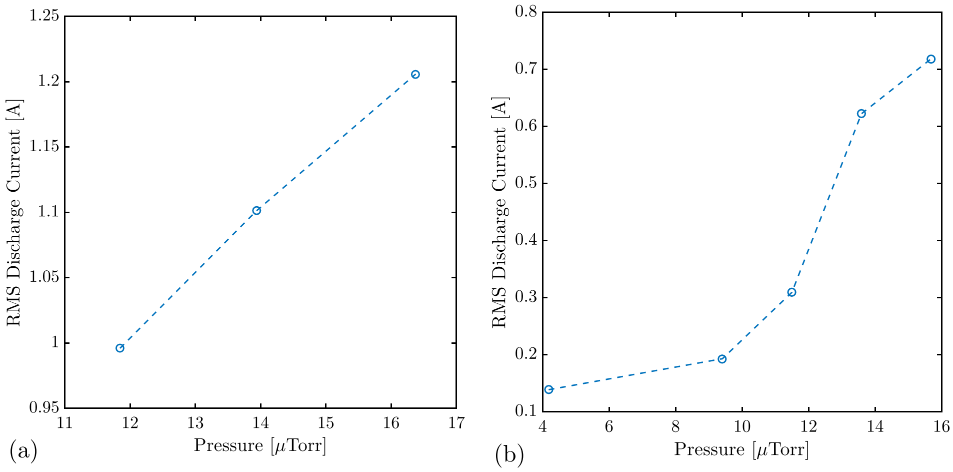


FIG. 10. RMS discharge current oscillations for the inner and outer channels of the X2. (a) RMS of the outer channel discharge current as a function of facility background pressure. Gas is injected via the inactive channel. (b) RMS of the inner channel discharge current as a function of facility background pressure. Gas is injected via the inactive channel.

performance is still an active area of research.[39] To provide context for our results, Figs. 10(a) and 10(b) show the root mean square (RMS) discharge current as a function of facility background pressure when increasing the mass flow through a non-operating channel. In these figures, we see that discharge oscillations increased monotonically with pressure, an effect that has been previously observed.[44] For typical Hall thruster discharge current oscillations, the empirical relationship $I_{pk-pk} \sim 6I_{rms}$ can be used as an estimate of the average peak-to-peak. Using this approximation to estimate the peak-to-peak oscillations during this experiment, we find that $I_{pk-pk} \sim 0.51I_{DC}$ for the inner channel and $I_{pk-pk} \sim 0.34I_{DC}$ for the outer. For reference, peak-to-peak discharge oscillations have been directly measured to exceed 100% of the mean current.[44] Since the literature is divided in its conclusions, we will neglect any contribution to the thrust due to discharge oscillations in our calculations. However, if the change in discharge oscillations between single and multi-channel modes were large, then this may be an additional process that affects the thrust from a NHT.

### F. Thrust increase

The expected increase in thrust due to both neutral ingestion [Eq. (5)] and divergence angle [Eq. (9)] changes is calculated to be $10.7 \pm 1.3$ mN. As seen in Fig. 11, these calculated increases account for the measured increase within uncertainty. The sum of the single channel thrusts is $340.8 \pm 4.5$ mN, the calculated dual channel thrust is $351.5 \pm 4.4$ mN, and the measured dual is $357.8 \pm 4.3$ mN. Of critical importance is that, based on the theory described in Sec. IV, the dual channel thrust and performance were accurately predicted within the uncertainty. This result suggests that local neutral ingestion and divergence angle are the dominant processes affecting nested Hall thruster performance. However, there are still other processes that could affect the performance to a lesser extent, such as plasma oscillations or cathode pressure gradients.

## VI. CONCLUSION

The nested Hall thruster is an attractive technology that scales Hall thrusters to higher power. These thrusters have shown that multi-channel operation leads to a synergy between channels improving the thrust over the sum of the individual channels. The total thrust for the conditions tested in this work increased by $17.0 \pm 6.2$ mN between dual-channel mode and single-channel with downstream injection summation at equal background pressure. Matching the background pressure using channel injection resulted in the thrust values being the same within uncertainty. Experimental evidence shows that the divergence of the ion beam is reduced because the higher local pressure causes a shift of the acceleration region upstream. This process is

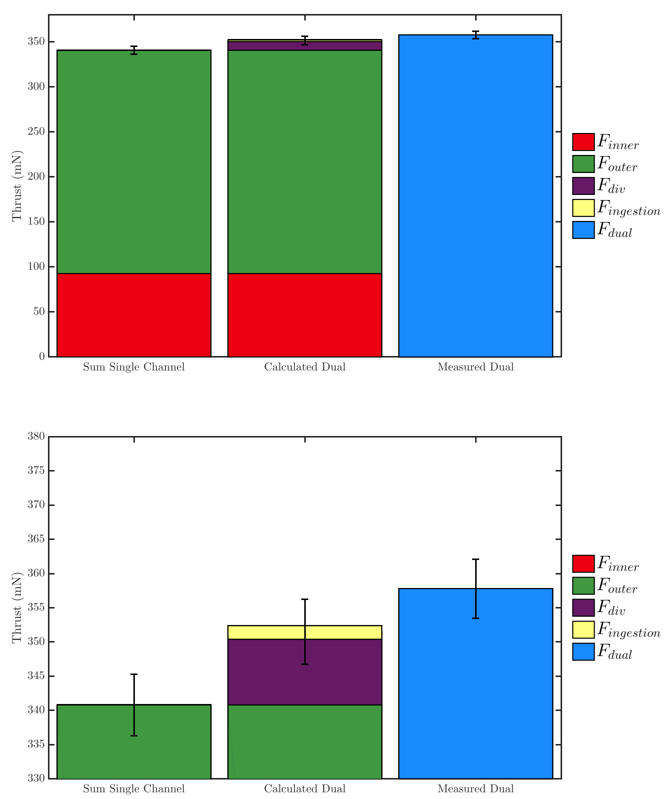


FIG. 11. Comparison of the sum of individual channel thrusts, the calculated dual channel thrust, and the measured dual channel thrust shows that the calculated value based on divergence and neutral ingestion models predicts the actual value within uncertainty. The top figure shows the full scale while the bottom shows a zoomed scale to visualize differences.

responsible for an 8.7 mN increase in thrust. Additionally, experiments suggests that the beam current is increased via neutral ingestion from the other channel. This process is responsible for 2.0 mN increase in thrust. Combining these two results, a $10.7 \pm 1.2$ mN increase in thrust would be expected. How interaction via plasma oscillations affects the dynamics of dual-channel operation was not quantified with the experimental techniques used in this work. The calculated increase in thrust agrees with the 17.0 mN measured increase suggesting that the theory described here accounts for the change in thrust for nested Hall thrusters. These processes detailed in the theory are a result of the nested design and are not a facility effect.

## ACKNOWLEDGMENTS

This work was funded in part by NASA Space Technology Research Fellowship Grants NNX15AQ43H, NNX15AQ37H, NNX13AL51H, and NNX14AL65H. The authors would like to thank Dr. Benjamin Jorns for his insightful discussions during the writing of this work.

[1]R. R. Hofer, D. Herman, J. E. Polk, H. Kamhawi, and I. G. Mikellides, "Development approach and status of the 12.5 kW HERMeS Hall thruster for the solar electric propulsion technology demonstration mission," in 34th International Electric Propulsion Conference, Hyogo-Kobe, Japan, IEPC-2015-186 (2015).
[2]R. R. Hofer, H. Kamhawi, I. G. Mikellides, D. A. Herman, J. E. Polk, W. Huang, J. Yim, J. Myers, and R. Shastry, "Design methodology and scaling of the 12.5 kW HERMeS Hall thruster for the solar electric propulsion technology demonstration mission," in 62nd JANNAF Propulsion Meeting, JANNAF-2015-3946, Nashville, TN (2015).
[3]D. M. Goebel and J. E. Polk, "Lanthanum hexaboride hollow cathode for the asteroid redirect robotic mission 12.5 kW Hall thruster," in 34th International Electric Propulsion Conference, Hyogo-Kobe, Japan, IEPC-2015-43 (2015).
[4]R. Liang, "The combination of two concentric discharge channels into a nested Hall-effect thruster," Ph.D. thesis (University of Michigan, Ann Arbor, MI, 2013).
[5]R. Florenz, "The X3 100-kW class nested-channel Hall thruster: Motivation, implementation, and initial performance," Ph.D. thesis (University of Michigan, Ann Arbor, MI, 2014).
[6]J. Brophy, R. Gershman, N. Strange, D. Landau, R. Merrill, and T. Kerslake, "300-kW solar electric propulsion system configuration for human exploration of near-earth asteroids," in 47th AIAA/ASME/SAE/ASEE Joint Propulsion Conference & Exhibit, San Diego, CA (American Institute of Aeronautics and Astronautics, 2011).
[7]R. R. Hofer and T. M. Randolph, "Mass and cost model for selecting thruster size in electric propulsion systems," J. Propul. Power **29**, 166–177 (2013).
[8]V. Zhurin, H. Kaufman, and R. Robinson, "Physics of closed drift thrusters," Plasma Sources Sci. Technol. **8**, R1 (1999).
[9]R. Spores, J. Monheiser, B. P. Dempsey, D. Wade, K. Creel, D. Jacobson, and G. Drummond, "A solar electric propulsion cargo vehicle to support NASA lunar exploration program," in 25th International Electric Propulsion Conference, Princeton, NJ, IEPC-2005-320 (2005), Vol. 31.
[10]R. Liang and A. D. Gallimore, "Far-field plume measurements of a nested-channel Hall-effect thruster," AIAA Paper 2011-1016, 2011.
[11]M. R. Nakles and W. A. Hargus, "Background pressure effects on ion velocity distribution within a medium-power Hall thruster," J. Propul. Power **27**, 737–743 (2011).
[12]M. L. R. Walker, "Effects of facility backpressure on the performance and plume of a Hall thruster," Ph.D. thesis (United States Air Force, 2005).
[13]T. Randolph, V. Kim, H. Kaufman, K. Kozubsky, V. V. Zhurin, and M. Day, "Facility effects on stationary plasma thruster testing," in *23rd International Electric Propulsion Conference IEPC-93-93* (1993), pp. 13–16.
[14]M. L. R. Walker, A. L. Victor, R. R. Hofer, and A. D. Gallimore, "Effect of backpressure on ion current density measurements in Hall thruster plumes," J. Propul. Power **21**, 408–415 (2005).
[15]D. L. Brown and A. D. Gallimore, "Evaluation of facility effects on ion migration in a Hall thruster plume," J. Propul. Power **27**, 573–585 (2011).
[16]R. R. Hofer and A. D. Gallimore, "The role of magnetic field topography in improving the performance of high-voltage Hall thrusters," AIAA Paper AIAA-2002-4111, 2002.
[17]I. D. Boyd, D. B. Van Gilder, and X. Liu, "Monte Carlo simulation of neutral xenon flows in electric propulsion devices," J. Propul. Power **14**, 1009–1015 (1998).
[18]G. A. Brid, *Molecular Gas Dynamics and the Direct Simulation of Gas Flows* (Oxford University Press, 1994).
[19]M. L. Walker and A. D. Gallimore, "Performance characteristics of a cluster of 5-kw laboratory Hall thrusters," J. Propul. Power **23**, 35–43 (2007).
[20]J. L. Rovey, M. L. Walker, A. D. Gallimore, and P. Y. Peterson, "Magnetically filtered faraday probe for measuring the ion current density profile of a Hall thruster," Rev. Sci. Instrum. **77**, 013503 (2006).
[21]R. J. Cedolin, W. A. Hargus, Jr., P. V. Storm, R. K. Hanson, and M. A. Cappelli, "Laser-induced fluorescence study of a xenon Hall thruster," Appl. Phys. B **65**, 459–469 (1997).
[22]J. W. A. Hargus and M. A. Cappelli, "Laser-induced fluorescence measurements of velocity within a Hall discharge," Appl. Phys. B **72**, 961–969 (2001).
[23]G. J. Williams, T. Smith, M. Domonkos, A. Gallimore, and R. Drake, "Laser-induced fluorescence characterization of ions emitted from hollow cathodes," IEEE Trans. Plasma Sci. **28**, 1664–1675 (2000).
[24]W. Huang, A. D. Gallimore, and T. B. Smith, "Two-axis laser-induced fluorescence of singly-charged xenon inside a 6-kW Hall thruster," in 49th AIAA Aerospace Sciences Meeting Including the New Horizons Forum and Aerospace Exposition, Orlando, Florida (2011).
[25]W. Huang, A. D. Gallimore, and T. B. Smith, "Interior and near-wall ion velocity distribution functions in the H6 Hall thruster," J. Propul. Power **29**, 1146–1154 (2013).
[26]S. Mazouffre, "Laser-induced fluorescence diagnostics of the cross-field discharge of Hall thrusters," Plasma Sources Sci. Technol. **22**, 013001 (2013).
[27]S. E. Cusson, E. T. Dale, and A. D. Gallimore, "Investigation of channel interactions in nested Hall thruster," J. Propul. Power **33**, 1037–1040 (2017).
[28]M. P. Georgin, V. Dhaliwal, and A. Gallimore, "Investigation of channel interactions in a nested Hall thruster part i: Acceleration region velocimetry," in *52nd AIAA/SAE/ASEE Joint Propulsion Conference* (2016), p. 5030.
[29]S. E. Cusson, E. T. Dale, and A. Gallimore, "Investigation of channel interactions in a nested Hall thruster part ii: Probes and performance," in *52nd AIAA/SAE/ASEE Joint Propulsion Conference* (2016), p. 5029.
[30]J. D. Frieman, T. M. Liu, and M. L. Walker, "Background flow model of Hall thruster neutral ingestion," J. Propul. Power **33**, 1087–1101 (2017).
[31]D. M. Goebel and I. Katz, *Fundamentals of Electric Propulsion: Ion and Hall Thrusters* (John Wiley & Sons, 2008), Vol. 1.
[32]B. M. Reid and A. D. Gallimore, "Near-field ion current density measurements of a 6-kW Hall thruster," in 31st International Electric Propulsion Conference, Ann Arbor, MI, IEPC-2009-124 (2009).
[33]R. R. Hofer, L. K. Johnson, D. M. Goebel, and R. E. Wirz, "Effects of internally mounted cathodes on Hall thruster plume properties," IEEE Trans. Plasma Sci. **36**, 2004–2014 (2008).
[34]R. R. Hofer, "Development and characterization of high-efficiency, high-specific impulse xenon Hall thrusters," Ph.D. thesis (University of Michigan, 2004).
[35]D. Gawron, S. Mazouffre, N. Sadeghi, and A. Héron, "Influence of magnetic field and discharge voltage on the acceleration layer features in a Hall effect thruster," Plasma Sources Sci. Technol. **17**, 025001 (2008).
[36]J.-P. Boeuf, "Tutorial: Physics and modeling of Hall thrusters," J. Appl. Phys. **121**, 011101 (2017).
[37]S. Mazouffre and G. Bourgeois, "Spatio-temporal characteristics of ion velocity in a Hall thruster discharge," Plasma Sources Sci. Technol. **19**, 065018 (2010).
[38]W. Huang, B. Drenkow, and A. Gallimore, "Laser-induced fluorescence of singly-charged xenon inside a 6-kW Hall thruster," AIAA Paper AIAA-2009-5355 (2009).
[39]M. J. Sekerak, A. D. Gallimore, D. L. Brown, R. R. Hofer, and J. E. Polk, "Mode transitions in Hall-effect thrusters induced by variable magnetic field strength," J. Propul. Power **32**, 903–917 (2016).

[40]J. Boeuf and L. Garrigues, "Low frequency oscillations in a stationary plasma thruster," J. Appl. Phys. **84**, 3541–3554 (1998).
[41]E. Choueiri, "Plasma oscillations in Hall thrusters," Phys. Plasmas **8**, 1411–1426 (2001).
[42]E. Chesta, C. M. Lam, N. B. Meezan, D. P. Schmidt, and M. A. Cappelli, "A characterization of plasma fluctuations within a Hall discharge," IEEE Trans. Plasma Sci. **29**, 582–591 (2001).
[43]M. S. McDonald and A. D. Gallimore, "Rotating spoke instabilities in Hall thrusters," IEEE Trans. Plasma Sci. **39**, 2952–2953 (2011).
[44]T. Randolph, V. Kim, H. Kaufman, K. Kozubsky, V. Zhurin, and M. Day, "Facility effects on stationary plasma thruster testing," in *23rd International Electric Propulsion Conference* (1993), pp. 13–16.